Molecular Dynamics Simulation of the Proline Conformational Equilibrium and Dynamics in Antamanide Using the CHARMM Force Field

Jürgen M. Schmidt,[†] Rafael Brüschweiler,[†,‡] Richard R. Ernst,[*,†] Roland L. Dunbrack, Jr.,[§] Diane Joseph,[§] and Martin Karplus[*,§]

Contribution from the Laboratorium für Physikalische Chemie, Eidgenössische Technische Hochschule, 8092 Zürich, Switzerland, and Department of Chemistry, Harvard University, Cambridge, Massachusetts 02138
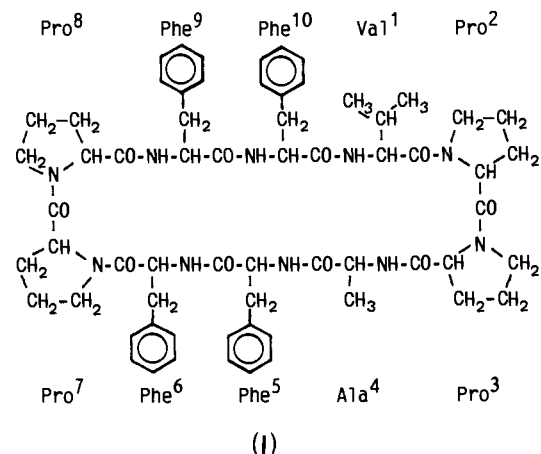
Received April 21, 1993[®]

Abstract: The recently developed atomic force field parameter set CHARMM 22.0.β is used for Langevin dynamics (LD) simulations that probe the motional characteristics of the four proline residues in the cyclic decapeptide antamanide in chloroform. Seven 2-ns trajectories were computed to sample the proline pucker motion for different backbone conformations. Most of the calculated $^3J_{HH}$ coupling constants and carbon-13 T_1 relaxation parameters, obtained by averaging over the conformations from the simulation data, are in nearly quantitative agreement with the experimental results obtained by NMR investigations of antamanide in chloroform solution (Mádi, Z. L.; Griesinger, C.; Ernst, R. R. *J. Am. Chem. Soc.* **1990**, *112*, 2908–2914). Within experimental accuracy, the equilibrium geometries deduced from NMR measurements are reproduced for all proline residues. Proline-2 and proline-7 sample two pucker conformations (C_β-*endo*/C_γ-*exo* and C_β-*exo*/C_γ-*endo*) on a picosecond time scale. In contrast, proline-3 and proline-8 are predominantly in the C_β-*exo*/C_γ-*endo* conformation with the endocyclic torsion angle χ_2 being negative, in agreement with experiment. The LD simulation indicates that the mobility of the proline ring moiety depends on the value of its ϕ dihedral angle, in accord with analyses based on structural data (Cung, M. T.; Vitoux, B.; Marraud, M. *New. J. Chem.* **1987**, *11*, 503–510). Comparison of the GROMOS united-atom potential results (Brunne, R. M.; van Gunsteren, W. F.; Brüschweiler, R.; Ernst, R. R. *J. Am. Chem. Soc.* **1993**, *115*, 4764–4768) with those from the CHARMM all-atom potential shows that both force fields represent adequately the equilibrium conformations while CHARMM 22 describes more accurately dynamic properties of the prolines in this system.

Introduction

The cyclic decapeptide antamanide (I) occurs in nature as a component of the poisonous mushroom *Amanita phalloides*.[1] It acts as an antidote against the phallotoxins that form a group of the poisonous components of this mushroom. The peptide bonds between Pro²–Pro³ and Pro⁷–Pro⁸ are cis, while Val¹–Pro² and Phe⁶–Pro⁷ are trans.[2] Although this restricts the motional freedom of the ring, it has been shown by X-ray diffraction[3] and NMR investigations[2,4–6] that antamanide adopts different backbone conformations in a crystalline environment and in solution. In chloroform solution, experimental data were found to be inconsistent unless multiple conformations were taken into account.[2,5,6] These results suggest that conformational variation occurs predominantly in the regions of the peptide links Ala⁴–Phe⁵ and Phe⁹–Phe¹⁰. Interconversion rates for such backbone transitions

have been determined by NMR experiments to be on the microsecond time scale.[7]

(I)

Recently, the analysis has been supplemented by a detailed NMR study of proton–proton coupling constants and carbon-13 longitudinal relaxation times on the proline residues of antamanide dissolved in chloroform[8] in analogy to earlier studies of cyclic tripeptides by Kessler et al.[9] The endocyclic dihedral angles of

* Correspondence addresses: Prof. Dr. R. R. Ernst, Laboratorium für Physikalische Chemie, Eidgenössische Technische Hochschule, ETH Zentrum, Universitätsstrasse 22, CH-8092 Zürich, Switzerland; Tel (+41)-1-H6324368, Fax (+41)-1-H6321021. Prof. Dr. M. Karplus, Harvard University, Department of Chemistry, 12 Oxford Street, Cambridge, MA 02138; Tel (617)-495-4018, Fax (617)-496-3204.

† Eidgenössische Technische Hochschule.

‡ Present address: Department of Molecular Biology, The Scripps Research Institute, 10666 North Torrey Pines Road, La Jolla, CA 92037.

§ Harvard University.

® Abstract published in *Advance ACS Abstracts*, August 15, 1993.

(1) Wieland, Th.; Faulstich, H. *Crit. Rev. Biophys.* **1978**, December, 185–260.

(2) Kessler, H.; Bats, J. W.; Lautz, J.; Müller, A. *Liebigs Ann. Chem.* **1989**, 913–928.

(3) Karle, I. L.; Wieland, T.; Schermer, D.; Ottenheym, H. C. J. *Proc. Natl. Acad. Sci. U.S.A.* **1979**, *76*, 1532–1536.

(4) Kessler, H.; Griesinger, C.; Lautz, J.; Müller, A.; van Gunsteren, W. F.; Berendsen, H. J. C. *J. Am. Chem. Soc.* **1988**, *110*, 3393–3396.

(5) Kessler, H.; Müller, A.; Pook, K.-H. *Liebigs Ann. Chem.* **1989**, 903–912.

(6) Brüschweiler, R.; Blackledge, M.; Ernst, R. R. *J. Biomol. NMR* **1991**, *1*, 3–11.

(7) Ernst, R. R.; Blackledge, M.; Boentges, S.; Briand, J.; Brüschweiler, R.; Ernst, M.; Griesinger, C.; Mádi, Z. L.; Schulte-Herbrüggen, T.; Sørensen, O. W. In *Proteins: Structure, Dynamics and Design*; Renugopalakrishnan, V., Carey, P. R., Smith, I. C. P., Huang, S. G., Storer, A. C., Eds.; ESCOM: Leiden, 1991; pp 11–28.

(8) Mádi, Z. L.; Griesinger, C.; Ernst, R. R. *J. Am. Chem. Soc.* **1990**, *112*, 2908–2914.

Table I. Dihedral Angles (in Degrees) of the Antamanide Starting Conformations Used in CHARMM Langevin Dynamics Simulations[a]

	ϕ	ψ	ω	χ_1	χ_2		ϕ	ψ	ω	χ_1	χ_2
simulation A[b]						simulation D[e]					
Val[1]	-112.9	158.1	177.5	64.0		Val[1]	-49.9	131.0	174.2	51.2	
Pro[2]	-63.9	161.2	2.4			Pro[2]	-63.6	144.3	2.0		
Pro[3]	-79.5	-20.5	-165.0			Pro[3]	-71.2	-19.2	-167.9		
Ala[4]	-103.4	-21.8	171.9			Ala[4]	-94.3	85.1	176.1		
Phe[5]	70.2	29.5	175.9	-51.9	-89.9	Phe[5]	-71.8	-13.3	-170.8	55.6	95.0
Phe[6]	-78.2	161.0	167.7	-70.1	-31.8	Phe[6]	-58.0	131.7	-175.9	-58.4	112.2
Pro[7]	-62.0	160.1	4.2			Pro[7]	-67.8	138.5	12.0		
Pro[8]	-91.8	-3.8	-176.9			Pro[8]	-104.6	24.0	-166.7		
Phe[9]	-101.1	-21.8	173.6	-69.5	168.7	Phe[9]	-83.8	-42.3	164.4	-60.1	111.5
Phe[10]	56.3	47.8	117.9	-49.5	-83.5	Phe[10]	71.2	-53.0	179.3	-96.7	-74.3
simulation B[c]						simulation E[e]					
Val[1]	-113.8	117.7	179.6	51.3		Val[1]	-115.8	137.6	-179.6	49.9	
Pro[2]	-57.6	132.8	-6.3			Pro[2]	-61.4	130.8	-4.0		
Pro[3]	-89.1	2.8	-176.2			Pro[3]	-87.9	-17.4	178.6		
Ala[4]	-90.2	87.9	-178.4			Ala[4]	-83.9	83.0	-178.5		
Phe[5]	-86.7	69.2	179.8	-66.9	-73.1	Phe[5]	-78.2	103.5	171.2	-71.3	-89.3
Phe[6]	-121.6	150.4	162.9	-64.5	115.3	Phe[6]	-146.0	142.3	178.4	-70.1	111.1
Pro[7]	-73.9	128.5	-13.2			Pro[7]	-52.8	130.0	-2.1		
Pro[8]	-91.0	-1.2	-178.0			Pro[8]	-89.2	-7.4	-166.2		
Phe[9]	-81.4	80.7	176.6	-60.2	104.8	Phe[9]	-104.7	80.6	171.4	69.3	-59.5
Phe[10]	-83.4	77.6	-174.6	-67.3	-77.7	Phe[10]	-80.7	68.4	-176.1	-44.2	88.3
simulation C[d]						simulation F[e]					
Val[1]	-6.8	103.7	-179.7	50.7		Val[1]	-105.5	130.4	169.2	67.4	
Pro[2]	-91.6	151.3	1.5			Pro[2]	-52.3	138.0	-26.3		
Pro[3]	-94.5	55.4	173.1			Pro[3]	-96.8	32.7	-174.4		
Ala[4]	-107.8	-50.7	170.1			Ala[4]	-80.7	-37.3	172.7		
Phe[5]	79.6	44.4	-178.7	-48.9	-67.6	Phe[5]	61.7	-57.3	-176.2	-87.3	-77.2
Phe[6]	-95.7	127.2	-178.7	-74.9	60.2	Phe[6]	-17.1	140.0	178.6	72.7	-84.9
Pro[7]	-94.1	152.5	0.8			Pro[7]	-62.0	137.6	-10.1		
Pro[8]	-94.7	55.4	177.8			Pro[8]	-107.5	54.6	179.5		
Phe[9]	-110.4	-56.4	168.5	-44.8	84.0	Phe[9]	-116.3	96.0	-158.3	-50.1	-69.4
Phe[10]	93.7	-24.0	174.9	-58.5	-62.0	Phe[10]	-105.1	57.7	-178.8	-77.7	84.6

[a] Classified according to the signs of the dihedral angles ϕ in residues 5 and 10, the backbone conformations are of type (+,+) for A and C and of type (-,-) for B and E, while conformations D and F represent types (-,+) and (+,-), respectively. In simulation G, coordinates identical to those in simulation C are used but with constraint terms imposed on ϕ_3 and ϕ_8 backbone dihedral angles (see text). Dihedral angles of proline side chains are omitted. Note that the default atom designations in GROMOS permute valine Cγ2 and Cγ1 with respect to the IUPAC–IUB recommendations (1970). To be consistent with the values reported in the various references, the valine χ_1 dihedral angle is given in terms of (N–Cα–Cβ–Cγ2), which differs from (N–Cα–Cβ–Cγ1) by approximately +120°. [b] The X-ray structure, heavy-atom Cartesian coordinates are taken from Karle et al.[3] [c] The MD⟨13–33⟩ structure, internal coordinates were taken from ref 5. [d] The conformation II obtained with the MEDUSA algorithm.[6] [e] Coordinates of the starting structures for simulations D–F were taken from a GROMOS simulation by Brunne et al.[13]

the proline side chain were found to exhibit considerable fluctuations on a time scale much shorter than that for the backbone torsional mode, i.e., on the order of a few tens of picoseconds. The rapid conformational interconversion leads to averaged NMR parameters for two (Pro[2] and Pro[7], see I) out of the four proline rings. Since the dynamics of interest is on the picosecond time scale, comparisons of the experimental results with molecular dynamics simulations can serve as a useful test of the latter, as well as an aid in the interpretation of the former.

We report on a series of Langevin dynamics (LD) simulations of antamanide in chloroform and examine the proline puckering (registry numbers: antamanide, 16898-32-1; proline, 147-85-3). We focus on the question of whether the force field parameters used and the simulations performed produce molecular motions in agreement with the experimental results. This kind of study could provide clues for a recalibration of the force field parameters in case of disagreements between simulation and experiment. Currently, various force fields are available which differ in their parameters and may lead to different dynamic properties. For the present investigation, we use the new all-atom force field[10,11] in CHARMM.[12] The reader is also referred to the results of a simultaneous investigation carried out by Brunne and co-workers,[13] who examined the standard GROMOS parameter set[14]

for the description of proline ring puckering. The results of the two sets of simulations are compared.

Computational Methods

Molecular dynamics (MD) simulations were initiated from various model structures differing in their backbone conformations which are listed in Table I. This was done to improve the sampling of the conformational space because the interconversion rate for different backbone conformations is slow on the time scale of the simulations. The crystal structure A was used with hydrogen atom extensions. Kessler and co-workers[2] derived a solution conformation B from vacuum MD simulations that included experimental distance restraints from the measurement of homonuclear nuclear Overhauser enhancement (NOE) effects. The structures A and B are also referred to as (+,+) and (-,-) conformations, respectively, to point out that the backbone dihedral angles ϕ_5 and ϕ_{10} adopt either positive or negative values. A third starting conformation C emerged from structure refinement procedures using the multiconformational search protocol MEDUSA.[6] Compared to the X-ray structure, a different hydrogen-bonding pattern is encountered in this latter structure, although it again has a (+,+) backbone conformation. Three further structures D, E, and F were intermediate conformations sampled from GROMOS MD trajectories being described by Brunne et al.[13] These latter structures represent (-,+), (-,-), and (+,-) backbone conformations, respectively. Finally, simulation G started from conformation C. It used constraint terms imposed on the proline backbone torsion angles ϕ_3 and ϕ_8 that confined their accessible conformational

(9) Kessler, H.; Friedrich, A.; Hull, W. E. *J. Org. Chem.* **1981**, *46*, 3892–3895. de Leeuw, F. A. A. M.; Altona, C.; Kessler, H.; Bermel, W.; Friedrich, A.; Krack, G.; Hull, W. E. *J. Am. Chem. Soc.* **1983**, *105*, 2237–2246.

(10) Dunbrack, R. L., Jr.; Joseph, D.; Karplus, M. To be published.

(11) MacKerell, A., Jr.; Karplus, M.; et al. To be published.

(12) Brooks, R. B.; Bruccoleri, R. E.; Olafson, B. D.; States, D. J.; Swaminathan, S.; Karplus, M. *J. Comput. Chem.* **1983**, *4*, 187–217.

(13) Brunne, R. M.; van Gunsteren, W. F.; Brüschweiler, R.; Ernst, R. R. *J. Am. Chem. Soc.* **1993**, *115*, 4764–4768.

(14) Van Gunsteren, W. F.; Berendsen, H. J. C. *Groningen Molecular Simulation (GROMOS) Library Manual*; Biomos: Groningen, The Netherlands, 1987.

Table II. Conformational Analysis of Proline Residues in Antamanide According to a Two-Site Jump Model[a]

	Pro²					Pro⁷					Pro³					Pro⁸			
		NMR		LD			NMR		LD			NMR		LD			NMR	LD	
	X-ray	1	2	1	2	X-ray	1	2	1	2	X-ray	1	2	1	2	X-ray	2	1	2
P	19.7	13	189	23.6 (9.3)	174.4 (4.2)	150.4	25	185	18.5 (10.2)	178.3 (2.4)	167.0	49	177	48.0 (8.8)	151.5 (5.8)	169.4	177	45.4 (4.4)	156.5 (2.2)
χ_{max}	26.8	46	32	38.3 (0.4)	35.8 (0.5)	12.2	46	34	38.3 (0.3)	36.1 (0.2)	30.7	42	46	40.1 (0.5)	38.5 (0.3)	32.4	42	40.0 (0.5)	38.6 (0.2)
χ_0	-1.1	4	-5	-3.8 (5.9)	-13.4 (2.1)	-9.6	-6	-8	-0.6 (6.5)	-11.3 (1.3)	-9.4	-24	-15	-19.6 (5.7)	-26.8 (2.8)	-16.3	-14	-18.1 (3.0)	-24.7 (1.2)
χ_1	-14.5	-30	23	-18.9 (4.8)	29.4 (0.7)	11.3	-22	26	-21.5 (4.6)	28.4 (0.6)	25.1	-4	35	-4.9 (5.4)	35.9 (0.8)	29.0	34	-6.6 (2.7)	35.8 (0.3)
χ_2	25.5	45	-32	33.1 (2.2)	-34.0 (0.8)	-10.7	42	-34	34.2 (1.3)	-34.4 (0.4)	-32.9	30	-42	25.5 (3.4)	-32.2 (1.6)	-31.3	-40	26.9 (1.5)	-34.0 (0.5)
χ_3	-26.5	-42	29	-34.8 (1.6)	25.8 (2.0)	5.9	-45	29	-34.1 (2.5)	27.3 (1.0)	26.8	-45	33	-36.3 (0.6)	16.3 (3.2)	22.8	31	-36.8 (0.4)	19.3 (1.2)
χ_4	15.2	24	-15	24.7 (4.6)	-8.1 (2.6)	3.0	31	-13	22.3 (5.7)	-10.4 (1.5)	-9.8	42	-11	35.6 (3.4)	6.6 (3.8)	-4.5	-10	35.0 (2.0)	3.3 (1.5)

[a] On the basis of the sign of the χ_2 dihedral angle that discriminates the two pucker states 1 and 2, mean pseudorotation phase angle P (deg), pucker amplitude χ_{max} (deg), and dihedral angles χ_i (deg) were calculated for the two states from six LD trajectories. Grand averages over the trajectories are given (standard deviations between the trajectories are given in parentheses). For comparison, experimental X-ray (from ref 3) and NMR-derived data (from ref 8) are included. Note that the numbering of the conformations of Pro³ and Pro⁸ is chosen here opposite to the one in refs 8 and 13 for reasons of consistency among the four proline residues.

Table III. Conformational Transition Analysis for Proline Residues in Antamanide According to a Two-Site Jump Model (JM)[a]

	no. of obsd transitions	p_1^{JM}	p_2^{JM}	p_1^{NMR}	p_2^{NMR}	τ_{R1}^{JM} (ps)	τ_{R2}^{JM} (ps)
Pro²	102 (63)	0.362 (0.159)	0.683	0.65	0.35	20.3 (16.4)	29.1 (10.6)
Pro⁷	71 (22)	0.498 (0.102)	0.502	0.55	0.45	29.6 (9.6)	29.9 (11.1)
Pro³	137 (49)	0.027 (0.011)	0.973	0.10	0.90	0.8 (0.7)	27.6 (10.8)
Pro⁸	102 (27)	0.024 (0.004)	0.976	0.00	1.00	0.9 (0.2)	36.5 (9.1)

[a] The sign of the χ_2 dihedral angle was used in conjunction with a threshold angle of 10° to discriminate the two pucker states $i = 1$ and 2 (see text). Pucker-state populations p_i and average residence times τ_{Ri}^{JM} were obtained as averages over six 2-ns LD trajectories (standard deviations between the trajectories are given in parentheses). NMR-derived data are given for comparison (from ref 8). Note that the numbering of the conformations of Pro³ and Pro⁸ is chosen here opposite to the one in refs 8 and 13 for reasons of consistency among the four proline residues.

space to the vicinity of the target values $\phi_{3,8} = -60°$. Force constants of 165 kJ mol⁻¹ rad⁻² are used for this purpose to allow the angles to vary by ±10° within an energy threshold of RT (2.5 kJ mol⁻¹ at a temperature of 300 K).

All reported LD simulations were performed with the CHARMM program including the refined force field parameter set of version 22.[11] The cyclic topology of antamanide was treated in an all-atom approach with explicit hydrogen atoms (162 total atoms). In a stochastic dynamics simulation protocol, random forces were applied to model the average effects of an apolar solvent environment. They were accounted for as friction and random terms[15] in the Langevin equation of motion,

$$m_i \dot{v}_i(t) = F_i(\{x_i(t)\}) - m_i \gamma_i v_i(t) + R_i(t) \qquad (1)$$

where m_i and v_i denote mass and velocity vectors of particle i. The force field F_i depends on the coordinates x_k of all particles, while the stochastic force $R_i(t)$ is assumed to be a stationary Gaussian random variable with zero mean and to show no correlation with prior steps:

$$\langle R_i(0) \ R_j(t) \rangle = 2m_i \gamma_i k_B T_{ref} \delta_{ij} \delta(t) \qquad (2)$$

where k_B and T_{ref} are the Boltzmann constant and the reference temperature of the bath, respectively. To each atom, a constant friction coefficient $\gamma_i = 19$ ps⁻¹ was assigned, which reflects the viscosity of the solvent chloroform.[16] Only the dynamic effects of the solvent were included; no correction for the change in the potential of mean force was used; an example where the latter correction was included in a Langevin

dynamics simulation is given in Levy et al.[17,18] A Verlet-type algorithm was employed for integrating eq 1,[19,20]

$$x_i(t_n + \Delta t) = \left\{ 2x_i(t_n) - x_i(t_n - \Delta t) + [F_i(t_n) + R_i(t_n)]m_i^{-1}(\Delta t)^2 + \frac{1}{2}\gamma_i \Delta t x_i(t_n - \Delta t) \right\}\left(1 + \frac{1}{2}\gamma_i \Delta t \right)^{-1} \qquad (3)$$

where n denotes the integration step number and Δt the step size. Initial velocity components were selected according to a Gaussian distribution function. A temperature of 300 K was maintained by coupling to the temperature bath via the stochastic term of eq 1. The SHAKE algorithm[21] was applied to keep all bond lengths constant, thus allowing for an increased integration step size of $\Delta t = 2$ fs. No cutoff radius was applied to Lennard-Jones and electrostatic potentials. The dielectric permittivity constant was chosen to be 1.

The conformations A and B were equilibrated using dihedral angle restraints on all torsional angles not involving hydrogen atoms during preparation periods of 100 ps. During this period, the restraining force constants were gradually reduced from the initial value of 165 kJ mol⁻¹ rad⁻² to 0. The other conformations were subjected to unrestrained equilibration at 50 K and then at 300 K for two successive 50-ps periods. The molecular dynamics simulations used for analysis were extended over 2 ns, each requiring 100 CPU h on a Sun SPARCstation 2.

In the analysis periods, the coordinates were sampled every 200 fs, yielding 10 000 conformations per trajectory. To eliminate overall translational and rotational contributions in the analysis of internal motion, the coordinate trajectories were postprocessed by aligning the principal axis system (PAS) of the molecular inertia tensor for every frame with a reference coordinate system. For the computation of NMR relaxation rate constants, the molecular rotation was reintroduced with the assumption that the rotational motion is isotropic.

Time correlation functions for CH directors were calculated by Fourier transform methods using the last 8000 coordinate sets in the trajectory. The correlation times for internal motion of the four prolines were determined by using an exponential fit of the first 512 points of the correlation functions, i.e., up to $\tau_{max} = 102.4$ ps. The Nelder–Mead simplex algorithm[22] has been employed for all nonlinear least-squares optimization tasks in the analysis procedures.

(15) Chandrasekar, S. *Rev. Mod. Phys.* **1943**, *15*, 1–89.

(16) Shi Yun-Yu; Wang, L.; van Gunsteren, W. F. *Mol. Simul.* **1988**, *1*, 369–383.

(17) Levy, R. M.; McCammon, J. A.; Karplus, M. *Chem. Phys. Lett.* **1979**, *65*, 4–11.

(18) Levy, R. M.; Karplus, M.; Wolynes, P. G. *J. Am. Chem. Soc.* **1981**, *103*, 5998.

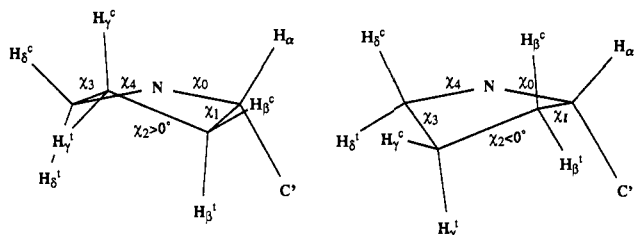(19) Brünger, A.; Brooks, C.; Karplus, M. *Chem. Phys. Lett.* **1984**, *105*, 495–500.

(20) Brooks, C.; Karplus, M.; Pettitt, B. M. In *Proteins: A Theoretical Perspective of Dynamics, Structure, and Thermodynamics*, Advances in Chemical Physics; Wiley: New York, 1985; Vol. 71.

(21) Ryckaert, J. P.; Cicotti, G.; Berendsen, H. J. C. *J. Comput. Phys.* **1977**, *23*, 327–341.

(22) Nelder, J. A.; Mead, R. *Comput. J.* **1965**, *7*, 308–313.

Figure 1. Designations for nuclei and angles in proline residues as used in the present text. The two pucker states are shown in schematic form. In the C_β-*endo*/C_γ-*exo* conformation (left), the χ_2 torsional angle is positive, while in the C_β-*exo*/C_γ-*endo* conformation (right), a negative χ_2 torsional angle is adopted. According to a different nomenclature, these states represent $^\gamma T_\beta$ and $_\gamma T^\beta$ twist conformations in which the pseudorotation phase P is approximately 0° and 180°, respectively.

Results

Three aspects of the trajectories of antamanide were analyzed for interpretation of the behavior of the molecule and for comparison with experiment. First, average proline pucker geometries were determined in conjunction with the computation of the number of pucker transitions and of the site-population ratios. Second, homonuclear $^3J_{HH}$ coupling constants were derived from the trajectories using extended Karplus relations. Finally, carbon-13 relaxation parameters were evaluated. Most of the results are given as grand averages over the six trajectories A-F with equal weights chosen to approximate a distribution of antamanide backbone conformations in solution. Such an averaging procedure incorporates some arbitrariness. However, because the variance of the parameters derived from the different trajectories is reasonably small (see e.g. Table III), the computed grand averages are representative.

Different conventions appear in the literature for the diastereotopic hydrogen positions as well as for the side-chain torsion angles of proline. For convenience, the nomenclature of Mádi and co-workers[8] is adopted here assigning methylene hydrogen atoms in the proline ring as cis and trans relative to H_α (not to be confused with cis and trans peptidyl bond conformation) and indicating the endocyclic torsion angles as χ_0–χ_4 (Figure 1). χ_0 thus replaces the backbone angle ϕ recommended by the IUPAC-IUB conventions,[23] from which it differs by an increment of approximately –60°.

Transition Analysis and Determination of Pucker Geometries. The geometry of the five-membered proline ring systems is described by two parameters, the maximum out-of-plane pucker amplitude χ_{max} and its position along the ring indicated by the pseudorotation phase P. Westhof and Sundaralingam[24] define the pseudorotation phase and amplitude as tan $P = B/A$ and $\chi_{max} = (A^2 + B^2)^{1/2}$, respectively, where

$$A = \frac{2}{5}\sum_{i=0}^{4}\chi_i \cos\left(\frac{4\pi}{5}(i-2)\right) \tag{4a}$$

$$B = -\frac{2}{5}\sum_{i=0}^{4}\chi_i \sin\left(\frac{4\pi}{5}(i-2)\right) \tag{4b}$$

In addition, 180° is added to the calculated P value whenever χ_2 shows a negative sign. The origin of the pseudorotation cycle ($P = 0°$) is chosen here to intersect the C_β–C_γ bond while a C_β-*endo*/C_γ-*exo* orientation is adopted. *Endo* and *exo* refer to the plane defined by C_δ–N–C_α and denote deflections of the respective carbons to the same and to the opposite side with respect to C'. The C_β-*endo*/C_γ-*exo* twist arrangement in which χ_2 has the
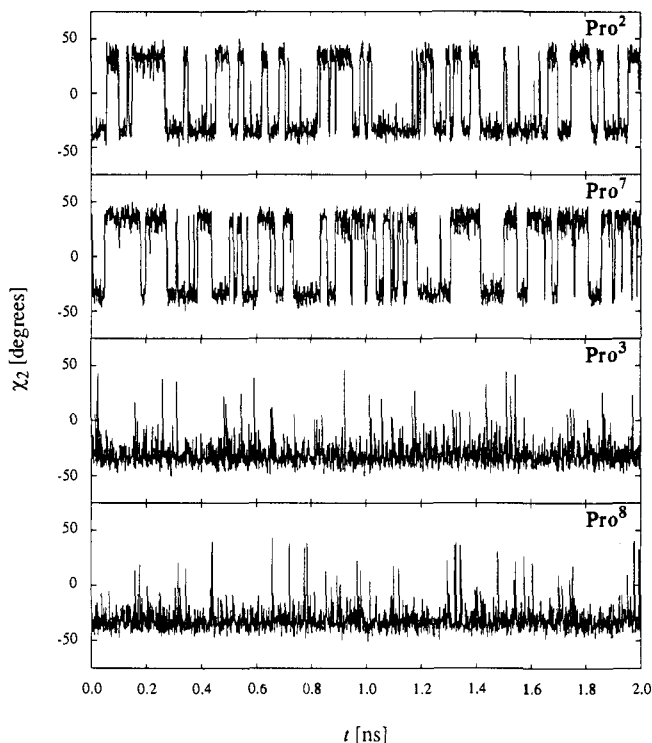
Figure 2. Proline χ_2 dihedral angle trajectories for the four proline residues from a LD simulation of antamanide. Samples from simulation A are plotted in increments of 1 ps.

maximum positive value is also referred to as the $^\gamma T_\beta$ conformation, while the mirror-image conformation C_β-*exo*/C_γ-*endo* is associated with the pseudorotation phase $P = 180°$ (maximum negative χ_2 value) and is denoted $_\gamma T^\beta$.

Individual time series were computed for the dihedral angles from the coordinate trajectories of Pro[2], Pro[3], Pro[7], and Pro[8]. Typical time courses of the torsion angles χ_2 are shown in Figure 2. It is evident from the figure that Pro[2] and Pro[7] are approximately equally distributed between two states, while Pro[3] and Pro[8] are essentially restricted to a single state, although there are rare, short-time excursions to a second state. The nature of these equilibria and their effects on the NMR parameters are discussed further below. In spite of these differences in the distributions, all proline residues sample two similar pucker states, as expected from the asymmetric constitution of the proline ring moiety.[24,25] Theoretical investigations[26,27] and statistical analyses[24] already point out that proline rings mainly adopt twist conformations close to the two geometries denoted $^\gamma T_\beta$ and $_\gamma T^\beta$. Since the χ_2 dihedral angle, together with χ_3, varies most during interconversion, proline ring conformations are distinguished by the sign of χ_2 and will henceforth be referred to as state 1 ($\chi_2 > 0$) and state 2 ($\chi_2 < 0$).

The results of the geometry analysis are presented in Table II. There is good overall agreement between the experimental and simulation results. For example, the χ_n (n = 0–4) values have signs and magnitudes that correspond to the estimates obtained from the NMR coupling constants. However, the simulations led in general to somewhat smaller pucker amplitudes χ_{max} and torsion angles χ_n, in particular for state 1 in Pro[2] and Pro[7]. The scatter plots of Figure 3 show that in the course of the trajectories these angles vary over a wide range which encloses the experimentally determined values. Simulated and experimental pseudorotation phases P agree within 15° for Pro[2] and Pro[7], while for the dominant conformation of Pro[3] and Pro[8] the values derived
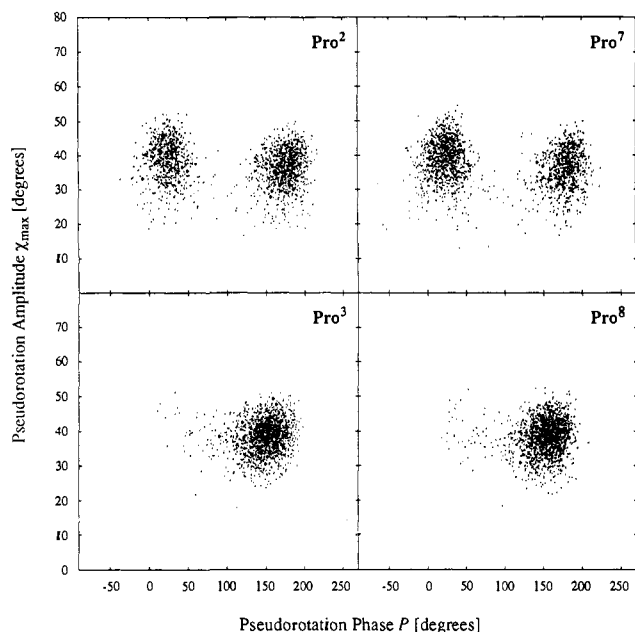
(23) IUPAC-IUB Commision on Biochemical Nomenclature. *Biochemistry* **1970**, *9*, 3471–3479.

(24) Westhof, G.; Sundaralingam, M. *J. Am. Chem. Soc.* **1983**, *105*, 970–976.

(25) Cung, M. T.; Vitoux, B.; Marraud, M. *New J. Chem.* **1987**, *11*, 503–510.

(26) London, R. E. *J. Am. Chem. Soc.* **1978**, *100*, 2678–2685.

(27) Shekar, S. C.; Easwaran, K. R. K. *Biopolymers* **1982**, *21*, 1479–1487.

MD Simulation of Proline Puckering

J. Am. Chem. Soc., Vol. 115, No. 19, 1993 8751

Figure 3. Scatter plots of pseudorotation parameters χ_{max} vs P for proline residues in a LD simulation of antamanide. Pucker parameters are plotted for the conformations of trajectory A at increments of 1 ps.

by simulation are 25° and 20° smaller than the experimental ones. Table II indicates that in the crystal structure there seem to be preferred states: state 1 for Pro² and state 2 for Pro⁷, Pro³, and Pro⁸, although it is expected that even in the crystal there is some dynamic conformational averaging of the proline rings.

To determine the pucker transition rate according to a two-site jump model, the positive and negative χ_2 angles were associated with the two sites, whereby the transient range is assigned to the preceding pucker conformation as long as χ_2 does not cross a ±10° barrier region. This threshold for defining a transition was derived from the fluctuation of various backbone dihedral angles. It accounts for local conformational jitter that does not correspond to a conformational transition. Average residence times τ_{Ri}^{JM} for the two pucker states $i = 1$ and 2 were calculated from the trajectories according to

$$\tau_{Ri}^{JM} = \frac{2}{n} p_i^{JM} T \qquad (5)$$

where p_i^{JM} denotes the probability of the state i within the total simulation time span T, and n is the number of observed transitions, so that $n/2$ is the occurrence number of a pucker state. The results of the transition analysis averaged over trajectories A–F are summarized in Table III. In LD simulations of antamanide, prolines 2 and 7 on the one hand and prolines 3 and 8 on the other hand behave similarly with respect to their dynamic properties. While the former two residues accommodate two pucker geometries with approximately equal probabilities, the corresponding populations are found to differ strongly in the case of the latter two residues (see also Figure 2). A marked preference for negative χ_2 torsional angles (state 2) is observed in Pro³ and Pro⁸, with the minor conformation (state 1) never exceeding 5% in population. The different behavior of prolines 2 and 7 vs 3 and 8 holds for all investigated backbone conformations (trajectories A–F) except for simulation G, in which the potentials had been modified to constrain $\phi_{3,8}$ near −60°. Interestingly, for Pro⁷, the probability p_1^{JM} was approximately 0.60 and 0.35 in symmetric (+,+) or (−,−) and asymmetric (+,−) or (−,+) antamanide backbone conformations, respectively. This indicates that there is a correlation with the backbone structure. For Pro², a large dispersion of the population ratios was observed on comparing different trajectories (p_1^{JM} = 0.39, 0.12, 0.41, 0.53, 0.50, and 0.22 for trajectories A–F, respectively). For Pro² in trajectories *B*

and *F*, the behavior is similar to that of Pro³ and Pro⁸; i.e., the first state has a small population.

Determination of $^3J_{HH}$ Coupling Constants. From the dihedral angles θ_{HH} of all H–C–C–H fragments, proton–proton J coupling values have been computed for each coordinate set on the trajectory and then averaged over the entire trajectory. A modified Karplus equation[28] was used, taking into account electronegativity effects of primary (α) and secondary (β) substituents:[29,30]

$$^3J_{HH} = a_1 \cos^2 \theta_{HH} + a_2 \cos \theta_{HH} + a_3 + \sum_i \Delta x_i^{group}\{a_4 + a_5 \cos^2(\xi_i \theta_{HH} + a_6|\Delta x_i^{group}|)\} \qquad (6a)$$

$$\Delta x_i^{group} = \Delta x_i^\alpha - a_7 \sum_i \Delta x_i^\beta \qquad (6b)$$

Appropriate coefficients a_1–a_7 have been given for HC–CH₂ and H₂C–CH₂ fragments by Haasnoot et al.[29] while relative electronegativity coefficients Δx_i for non-hydrogen atoms were taken from Huggins.[31] The coefficient ξ_i takes the values ±1 depending on the orientation of the substituent i as discussed by Haasnoot et al.[30]

Results are given in Table IV for the grand averages (i.e., averages over trajectories A–F with equal weights). For Pro³ and Pro⁸, the large difference in the $^3J_{HH}$ coupling constants for different HH pairs confirms a predominantly rigid ring conformation. Conformational averaging is responsible for the reduced range of the $^3J_{HH}$ coupling constants in Pro² and Pro⁷. Most of the calculated J coupling constants agree well with the experimental values. However, some of them deviate more than 1.5 Hz (see underlined values in Table IV).

For Pro³ and Pro⁸, the deviations parallel approximately the deviations between the experimental and computed pseudorotation phase. From the calculations of Haasnoot et al.,[29] the variation in the $^3J_{HH}$ coupling constants with the dihedral angle can be related to the pseudorotation phase. The slope of this variation is given in Table IV by the signs of the derivatives of the $^3J_{HH}$ coupling constants with respect to the pseudorotation phases P_i of the two pucker states. Similarly, the dependence on the population p_1 is indicated. A "0" indicates no significant sensitivity to the respective parameter. The indicated variability applies to the entire range of accessible parameter values: $0° \leq P_1 \leq 50°$, $130° \leq P_2 \leq 180°$, $35° \leq \chi_{max}^{(1,2)} \leq 45°$. This information was derived from the Figure 4 given in Haasnoot et al.[30]

For Pro³ and Pro⁸, which are essentially in the pure $i = 2$ state ($\chi_2 < 0$, $P = 150$–$180°$), the analysis is relatively straightforward. There are three small coupling constants ($H_\alpha H_{\beta^t}$, $H_{\beta^t} H_\gamma^c$, $H_\gamma^c H_{\delta^t}$) whose values are insensitive to the pseudorotation parameter P_2 in this region. There are three coupling constants that are calculated to be too small ($H_\alpha H_{\beta}^c$, $H_{\beta}^c H_\gamma^t$, $H_\gamma^t H_{\delta}^c$), which all increase with increasing pseudorotation phase between 150° and 180°, and four coupling constants which are calculated to be too large ($H_{\beta}^c H_\gamma^c$, $H_{\beta}^t H_\gamma^t$, $H_\gamma^c H_{\delta}^c$, $H_\gamma^t H_{\delta}^t$), which all decrease with increasing pseudorotation phase in this range. Thus, an increase of the computed pseudorotation phase P_2 by ~20° toward the experimental value would significantly improve almost all of the computed J values.

As Haasnoot and co-workers[30] also pointed out, five out of the ten possible three-bond couplings, namely, those in which the coupled protons are *trans*-oriented with respect to the ring plane, are sensitive to changes in the pucker geometry. In a dynamic equilibrium, the effective pucker geometry can be altered by changing the weights associated with each structure, rather than

(28) Karplus, M. *J. Am. Chem. Soc.* **1963**, *85*, 2870–2871.
(29) Haasnoot, C. A. G.; DeLeeuw, F. A. A. M.; Altona, C. *Tetrahedron* **1980**, *36*, 2783–2792.
(30) Haasnoot, C. A. G.; DeLeeuw, F. A. A. M.; DeLeeuw, H. P. M.; Altona, C. *Biopolymers* **1981**, *20*, 1211–1245.
(31) Huggins, M. L. *J. Am. Chem. Soc.* **1953**, *75*, 4123–4126.

8752 *J. Am. Chem. Soc., Vol. 115, No. 19, 1993*

Schmidt et al.

Table IV. Calculated Average H,H Dihedral Angles θ_{HH} and $^3J_{HH}$ Coupling Constants for Proline Residues in Antamanide Based on the Two-Site Jump Model (JM) Together with Experimental $^3J_{HH}$ Values (from Ref 8)[a]

	$\dfrac{\partial J}{\partial p_1}$	$\dfrac{\partial J}{\partial P_1}$	$\dfrac{\partial J}{\partial P_2}$	Pro^2			Pro^7			Pro^3			Pro^8		
				θ^{JM}_{HH} (deg)	J^{JM}_{HH} (Hz)	J^{NMR}_{HH} (Hz)	θ^{JM}_{HH} (deg)	J^{JM}_{HH} (Hz)	J^{NMR}_{HH} (Hz)	θ^{JM}_{HH} (deg)	J^{JM}_{HH} (Hz)	J^{NMR}_{HH} (Hz)	θ^{JM}_{HH} (deg)	J^{JM}_{HH} (Hz)	J^{NMR}_{HH} (Hz)
$H_\alpha H_\beta^c$	0	+	+	8.6	7.7	8.0	-0.7	7.6	8.8	36.3	6.8	8.5	36.3	6.8	8.1
$H_\alpha H_\beta^t$	+	-	0	-112.0	4.3	7.4	-121.4	5.6	5.8	-83.8	1.4	1.1	-83.9	1.4	0.9
$H_\beta^c H_\gamma^c$	0	+	-	-10.6	7.5	7.1	-0.2	7.4	7.4	-33.8	8.0	6.8	-36.1	7.6	6.8
$H_\beta^c H_\gamma^t$	-	0	+	-131.0	8.1	4.8	-120.8	6.5	5.9	-153.2	11.4	12.0	-155.2	11.9	13.0
$H_\beta^t H_\gamma^c$	+	-	0	106.9	4.7	9.0	117.1	6.2	7.5	84.1	1.0	2.4	81.9	1.0	1.4
$H_\beta^t H_\gamma^t$	0	+	-	-14.1	7.4	7.1	-4.0	7.4	7.0	-36.6	7.4	6.5	-39.0	7.0	6.4
$H_\gamma^c H_\delta^c$	0	+	-	4.1	7.6	7.6	-3.7	7.3	7.3	14.6	9.1	7.6	18.5	8.8	7.3
$H_\gamma^c H_\delta^t$	+	-	0	-115.8	5.0	8.5	-123.0	6.3	7.4	-105.0	2.7	2.1	-101.2	2.2	1.5
$H_\gamma^t H_\delta^c$	-	0	+	124.9	6.7	4.6	117.2	5.7	5.4	135.2	7.5	10.3	139.3	8.3	10.9
$H_\gamma^t H_\delta^t$	0	+	-	4.1	7.7	7.0	-3.5	7.3	7.0	15.5	9.3	8.5	19.5	9.1	8.8

[a] Discrepancies between simulation and experimental data of 1.5 Hz or more are underlined. The dependence of the average $^3J_{HH}$ coupling constant on the population p_1 (with $p_2 = 1 - p_1$) and on the pseudorotation phases P_1 and P_2 is indicated; "+" and "-" denote positive and negative values for the derivative, respectively, while "0" indicates no significant sensitivity to the respective parameter.

by changing the pseudorotation phase in each. The larger deviation from experiment in the case of Pro^2 in comparison to Pro^7, which yields very good coupling constant values, is likely to be due to the larger calculated difference in the populations of the two pucker states for Pro^2 than for Pro^7. It should be noted, however, that this argument is somewhat circular since the experimental data for the populations come from fitting the coupling constants.

Determination of $^{13}C\ T_1$ Relaxation Parameters and Correlation Times of Internal Motion. Carbon-13 T_1 relaxation times at a resonance frequency of 100 MHz are governed predominantly by dipolar interactions between the carbon and directly bonded hydrogen spins. They depend on contributions from the overall tumbling and from internal motion with individual correlation times τ_c and τ_{int}, respectively. Different motional models can be used and the results applied to the analysis of the simulations.[18]

In a first approach, we consider the internal motion as a two-site jump process (JM) between the two pucker states associated with probabilities p_1^{JM} and p_2^{JM}.[8,25] The relaxation rate constant is given by

$$(T_1^{JM})^{-1} = S_f^2(JM)\{[1-3p_1^{JM}p_2^{JM}\sin^2\Delta\theta^{JM}]T_1^{-1}(\tau_c) + $$
$$[3p_1^{JM}p_2^{JM}\sin^2\Delta\theta^{JM}]T_1^{-1}(\tau_{tot}^{JM})\} \quad (7)$$

where

$$(\tau_{tot}^{JM})^{-1} = \tau_c^{-1} + (\tau_{int}^{JM})^{-1} \quad (8)$$

and $\Delta\theta^{JM}$ is the change in the orientation of a CH bond vector caused by a ring-puckering transition. The function $T_1^{-1}(\tau)$ is represented in terms of the spectral densities $J(\omega,\tau)$ by the well-known expression

$$T_1^{-1}(\tau) = \frac{\gamma_H^2\gamma_C^2\hbar^2 N}{40\pi^2 r_{CH}^6}\left(\frac{\mu_0}{4\pi}\right)^2\left\{\frac{3}{2}J(\omega_0^C,\tau) + \frac{1}{2}J(\omega_0^C-\omega_0^H,\tau) + \frac{6}{2}J(\omega_0^C+\omega_0^H,\tau)\right\} \quad (9)$$

with

$$J(\omega,\tau) = \frac{2\tau}{1 + (\omega\tau)^2} \quad (10)$$

where N denotes the number of hydrogen atoms attached to the considered carbon and r_{CH} is the internuclear distance, typically set to 1.08 Å. The order parameter $S_f^2(JM)$[32] takes into account the averaging of the dipolar interaction by fast angular oscillations of the CH vectors within each of the potential energy wells of the

(32) Clore, G. M.; Szabo, A.; Bax, A.; Kay, L. E.; Driscoll, P. C.; Gronenborn, A. M. *J. Am. Chem. Soc.* **1990**, *112*, 4989–4991.

Table V. CH Bond Reorientation in Proline Residues in Antamanide According to a Two-Site Jump Model (JM)[a]

	$\Delta\theta^{JM}$ (deg)	$\Delta\theta^{NMR\ b}$ (deg)	τ_{int}^{JM}(ps)	τ_{int}^{NMRb}(ps)	S_s^2(JM)	S_f^2(JM)
Pro^2			11.1 (7.4)	30		
$C_\alpha H$	5.2(3.1)	4			0.94 (0.02)	0.90 (0.04)
$C_\beta H$	52.3 (5.0)	50			0.62 (0.12)	0.84 (0.03)
$C_\gamma H$	69.1 (5.3)	75			0.55 (0.14)	0.82 (0.04)
$C_\delta H$	30.7 (1.7)	35			0.80 (0.04)	0.78 (0.05)
Pro^7			14.4 (4.0)	36		
$C_\alpha H$	3.8 (1.3)	1			0.95 (0.01)	0.92 (0.02)
$C_\beta H$	53.4 (3.6)	44			0.52 (0.06)	0.85 (0.02)
$C_\gamma H$	73.7 (6.7)	76			0.41 (0.16)	0.84 (0.03)
$C_\delta H$	32.4 (1.3)	41			0.79 (0.01)	0.79 (0.04)
Pro^3			0.8 (0.7)	nd		
$C_\alpha H$	3.3 (2.4)	nd			1.00 (0.00)	0.84 (0.04)
$C_\beta H$	42.1 (6.0)	nd			0.96 (0.03)	0.86 (0.03)
$C_\gamma H$	60.7 (4.2)	nd			0.94 (0.03)	0.79 (0.04)
$C_\delta H$	28.6 (2.3)	nd			0.98 (0.01)	0.79 (0.02)
Pro^8			0.9 (0.2)	nd		
$C_\alpha H$	3.6 (2.4)	nd			1.00 (0.00)	0.88 (0.02)
$C_\beta H$	43.5 (3.5)	nd			0.97 (0.01)	0.89 (0.01)
$C_\gamma H$	63.5 (2.5)	nd			0.94 (0.01)	0.82 (0.01)
$C_\delta H$	31.8 (1.7)	nd			0.98 (0.00)	0.82 (0.01)

[a] The reorientation angles $\Delta\theta^{JM}$ were calculated as the angles between the mean CH bond vectors of the two pucker states documented in Table II. The correlation times τ_{int}^{JM} were calculated on the basis of eqs 5 and 11 (see text). For comparison with the correlation function model, the order parameters S_f^2(JM) and S_s^2(JM) were computed from eqs 12 and 13, given p_1^{JM}, p_2^{JM}, and $\Delta\theta^{JM}$ obtained from the trajectory. Grand averages over six LD trajectories are given (standard deviations between the trajectories in parentheses). [b] Experimental values from ref 8; nd, not determined.

two pucker states. The behavior observed here is related in character to that observed in model LD simulations of ^{13}CH relaxation of aliphatic side chains.[17,18] There, a subpicosecond relaxation ($\sim$0.1 ps) due to oscillations within a rotamer well was followed by a much slower relaxation ($\sim$100 ps) corresponding to transitions between wells. In the present case, the short-time relaxation behavior is similar, but the slow relaxation process is faster because the proline pucker barrier is significantly lower.[10]

The angles $\Delta\theta^{JM}$, which are given in Table V, were calculated as differences between the average pucker geometries of states $i = 1$ and 2 obtained from the PAS-oriented MD trajectories. For Pro^2 and Pro^7, to which this jump model is applicable, the values of $\Delta\theta$ obtained from NMR analysis ($\Delta\theta^{NMR}$ in Table V) are in good accord with the simulation results. The correlation time τ_{int}^{JM} can be obtained from the individual state residence times

τ_{R1}^{JM} and τ_{R2}^{JM}:[26]

$$(\tau_{int}^{JM})^{-1} = (\tau_{R1}^{JM})^{-1} + (\tau_{R2}^{JM})^{-1} \quad (11)$$

The local motion order parameters $S_f^2(JM)$ were computed separately for the two pucker states. For this purpose, each of the six trajectories was divided into segments with $\chi_2(t) > 0$ (state 1) and $\chi_2(t) < 0$ (state 2). For the two states, the average orientation angles $\bar{\theta}_i$, $i = 1$ and 2, were determined for each CH vector. The deviation fluctuations of the orientation angle $\theta(t)$ from $\bar{\theta}_i$ within the time segment associated with state i define then the local motion order parameter of a particular CH vector according to

$$S_f^2(JM) = \sum_{i=1}^{2} p_i^{JM}\frac{1}{4}\overline{\{3\cos^2(\theta(t)-\bar{\theta}_i) - 1\}^2} \quad (12)$$

The values given in Table V are grand averages over the six trajectories and over the two CH vectors of each geminal pair. Provided that the CH vectors move within a cone of rotational symmetry, this procedure of calculation of $S_f^2(JM)$ is equivalent to the more traditional expression

$$S_f^2(JM) = \sum_{i=1}^{2} p_i^{JM} \langle P_2(\cos\theta_{\alpha\beta}^{(i)}) \rangle$$

$$= \sum_{i=1}^{2} p_i^{JM} \sum_{\alpha,\beta} p_\alpha p_\beta P_2(\cos\theta_{\alpha\beta}^{(i)}) \quad (12a)$$

where α and β index all possible orientations that the CH vector can assume with the probabilities p_α and p_β, and where $\theta_{\alpha\beta}^{(i)}$ is the difference angle within all possible pairs of orientations.[33] $P_2(x)$ denotes as usual the second-rank Legendre polynomial.

For comparison with the correlation function model discussed below, it is possible to identify the first bracket in eq 7 with the slow motion internal order parameter $S_s^2(JM)$:

$$S_s^2(JM) = 1 - 3p_1^{JM}p_2^{JM}\sin^2\Delta\theta^{JM} \quad (13)$$

This quantity is also included in Table V.

In a more general model-free approach, which does not require the discrimination of pucker states, the reorientation of the proline CH vectors in the PAS is described by the time correlation function $C(\tau)$ according to Lipari and Szabo,[33]

$$C(\tau) = \langle P_2(\mathbf{e}(t+\tau)\cdot\mathbf{e}(t)) \rangle_t \quad (14)$$

where $\mathbf{e}(t)$ denotes the time-dependent unit vector along the CH bond. The averaging is over the time t along the trajectory, as indicated by the brackets $\langle\ \rangle_t$. For explicit calculations, the correlation functions are parametrized in terms of correlation times τ_{int}^{CF} and order parameters $S^2(CF)$.
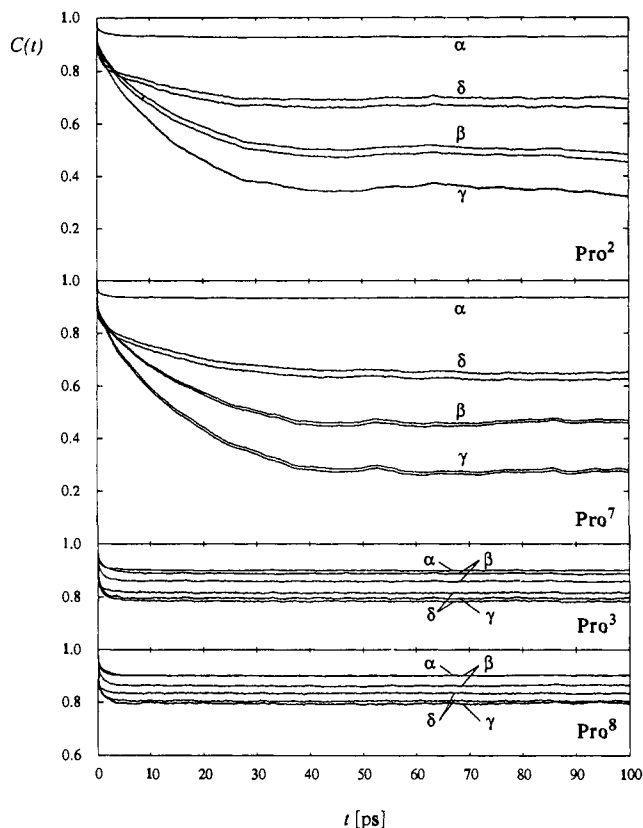
The correlation functions $C(\tau)$ shown in Figure 4 cannot be described by a single-exponential form, due to the presence of rapid and slow intramolecular processes as expected from Table V, and an extended expression had to be chosen:

$$C(\tau) = \{S_f^2(CF) + [1 - S_f^2(CF)]e^{-t/\tau^{CF}_{int,f}}\}\{S_s^2(CF) +$$
$$[1 - S_s^2(CF)]e^{-t/\tau^{CF}_{int,s}}\} \quad (15)$$

with $S_f^2(CF)$ and $\tau_{int,f}^{CF}$ referring to fast vibrational modes and $S_s^2(CF)$ and $\tau_{int,s}^{CF}$ to the slower puckering process. NMR relaxation at Larmor frequencies of several hundred megahertz is not sensitive to the rapid process with $\tau_{int,f}^{CF}$ in the subpicosecond range, and it is allowed to approximate $C(\tau)$ for longer times by

$$C(\tau) = S_f^2(CF)\{S_s^2(CF) + [1 - S_s^2(CF)]e^{-t/\tau^{CF}_{int}}\} \quad (16)$$

In the representation of Figure 4, the rapid process appears as

(33) Lipari, G.; Szabo, A. *J. Am. Chem. Soc.* **1982,** *104,* 4546–4559.

Figure 4. Time correlation functions calculated for the reorientation of the CH bond vectors in the proline residues of antamanide. The examples were derived from simulation A.

a steep falloff within the first few points. This correlation function, combined with the contribution for overall molecular tumbling, leads to the following expression for the longitudinal relaxation rate constant:

$$(T_1^{CF})^{-1} = S_f^2(CF)\{S_s^2(CF)T_1^{-1}(\tau_c) + [1 - S_s^2(CF)]T_1^{-1}(\tau_{tot}^{CF})\} \quad (17)$$

with $(\tau_{tot}^{CF})^{-1} = \tau_c^{-1} + (\tau_{int}^{CF})^{-1}$ and $T_1^{-1}(\tau)$ from eq 9.

From geometric restrictions, pairwise similar correlation functions are expected for CH pairs belonging to the same methylene group and indeed were found. For this reason, pair averages are given in Table VI for the internal correlation times τ_{int}^{CF} and order parameters $S_s^2(CF)$ and $S_f^2(CF)$ of $C_\beta H$, $C_\gamma H$, and $C_\delta H$.

For comparison with the two-site jump-model analysis discussed above, the order parameters $S_s^2(CF)$ from the correlation function analysis were interpreted, on the basis of eq 13, in terms of pucker reorientation angles, which we designate $\Delta\theta^{CF}$. The populations p_1^{JM} and p_2^{JM}, needed to evaluate $\Delta\theta^{CF}$, are taken from the two-site jump-model analysis. The resulting reorientation angles are listed also in Table VI. The $\Delta\theta^{CF}$ values obtained for $C_\beta H$, $C_\gamma H$, and $C_\delta H$ bond reorientation in Pro^2 and Pro^7 agree well with $\Delta\theta^{NMR}$ and $\Delta\theta^{JM}$ (Table V). Those for $C_\alpha H$ are too large due to the difficulty of separating S_s^2 and S_f^2 values that are close to 1. No meaningful $\Delta\theta^{CF}$ values can be obtained for Pro^3 and Pro^8, whose motion is essentially limited to a single well.

The intramolecular ring puckering correlation times τ_{int}^{JM} (Table V) and τ_{int}^{CF} (Table VI), determined from the same LD trajectories, are consistent among themselves for the mobile $C_\beta H_2$, $C_\gamma H_2$, and $C_\delta H_2$ groups of Pro^2 and Pro^7. The shorter correlation times for C_α and for Pro^3 and Pro^8, which are predominantly due to local motion, show a larger spread accompanied with wide error limits. However, the results of the two-site jump model and of the correlation function analysis do not differ significantly.

Table VI. Analysis of the Time Correlation Functions of CH Bond Reorientation According to the Correlation Function Model (CF)[a]

	S_s^2(CF)	S_f^2(CF)	τ_{int}^{CF} (ps)	$\tau_{int}^{NMR\ b}$ (ps)	$\Delta\theta^{CF}$ (deg)	$\Delta\theta^{NMR\ b}$ (deg)
Pro^2				30		
C$_\alpha$H	0.94 (0.04)	0.97 (0.02)	3.7 (2.7)		18.1 (6.5)	4
C$_\beta$H	0.58 (0.15)	0.89 (0.03)	12.6 (7.0)		50.3 (5.1)	50
C$_\gamma$H	0.43 (0.19)	0.88 (0.03)	12.5 (6.9)		6.3 (5.2)	75
C$_\delta$H	0.78 (0.05)	0.85 (0.02)	10.9 (5.4)		33.3 (4.7)	35
Pro^7				36		
C$_\alpha$H	0.97 (0.01)	0.95 (0.01)	3.8 (2.9)		11.9 (2.5)	1
C$_\beta$H	0.49 (0.05)	0.87 (0.03)	14.2 (4.3)		51.3 (3.7)	44
C$_\gamma$H	0.30 (0.03)	0.92 (0.06)	15.6 (7.5)		75.0 (5.6)	76
C$_\delta$H	0.74 (0.02)	0.83 (0.02)	19.8 (9.9)		32.9 (1.4)	41
Pro^3				nd		
C$_\alpha$H	0.90 (0.02)	0.95 (0.02)	4.5 (3.8)		nd	nd
C$_\beta$H	0.89 (0.01)	0.95 (0.03)	2.8 (2.8)		nd	nd
C$_\gamma$H	0.81 (0.02)	0.93 (0.06)	2.4 (3.0)		nd	nd
C$_\delta$H	0.82 (0.02)	0.95 (0.05)	1.8 (1.9)		nd	nd
Pro^8				nd		
C$_\alpha$H	0.92 (0.01)	0.96 (0.02)	3.5 (3.5)		nd	nd
C$_\beta$H	0.90 (0.01)	0.97 (0.02)	1.5 (1.3)		nd	nd
C$_\gamma$H	0.83 (0.03)	0.95 (0.04)	1.5 (1.3)		nd	nd
C$_\delta$H	0.84 (0.03)	0.96 (0.04)	1.3 (1.6)		nd	nd

[a] Internal motion correlation times τ_{int}^{CF} and order parameters S_s^2 and S_f^2 were obtained by least-squares fitting the correlation functions according to eq 16. The pucker reorientation angles $\Delta\theta^{CF}$ were calculated from S_s^2(CF) by eq 13 using the state probabilities p_i^{JM} taken from the two-site jump model. All quantities are given as averages over six trajectories (standard deviations between the trajectories in parentheses). [b] Experimental values from ref 8; nd, not determined.

On the basis of the MD trajectories, carbon-13 T_1 relaxation times were computed following the two described approaches. In the framework of the two-site jump model, the parameters p_1^{JM}, p_2^{JM}, $\Delta\theta^{JM}$, τ_{int}^{JM}, and S_f^2(JM) computed from the trajectories were inserted into eq 7. The missing overall rotational correlation time τ_c was optimized by least-squares fitting the computed values NT_1^{JM} to the experimental NT_1^{exp} values, both given in Table VII. In an analogous manner, the parameters S_s^2(CF), S_f^2(CF), and τ_{int}^{CF}, computed from the correlation function model, were inserted into eq 17 for T_1^{CF}. Again, the molecular tumbling correlation time τ_c was optimized by a least-squares procedure applied to the NT_1^{CF} values. The correlation times τ_c obtained, 190 and 184 ps for the two-site jump and correlation function models, respectively, are in good agreement with that deduced for antamanide in chloroform solution ($\tau_c = 180$ ps).[36] The analysis yields NT_1 values for the carbons in Pro^2 and Pro^7 in good agreement with experiment (Table VII) and supports the internal motional behavior derived from the simulations. For Pro^3 and Pro^8, the weak tendency of longer NT_1^{exp} values for C$_\beta$ and C$_\gamma$ in comparison to C$_\alpha$ and C$_\delta$ is barely recognizable in the computed values. It seems that the flexibility of Pro^3 and Pro^8 is slightly underestimated by the CHARMM force field.

Discussion

The results of the Langevin dynamics simulation are in nearly quantitative agreement with the NMR parameters that have been measured for the proline residues in antamanide. The study confirmed that Pro^2 and Pro^7 interconvert between two pucker conformations, while Pro^3 and Pro^8 strongly prefer one conformation. The computed conformational dynamics of Pro^2 and Pro^7, i.e. the magnitudes of the internal correlation times ($\tau_{int} = 10$–20 ps), obtained from analyses of both the two-site jump-model and the time correlation functions for CH bond reorien-

(34) Sarkar, S. K.; Torchia, D. A.; Kopple, K. D.; Van der Hart, D. L. *J. Am. Chem. Soc.* **1984**, *106*, 3328–3331.
(35) DeTar, D. F.; Luthra, N. *J. Am. Chem. Soc.* **1977**, *99*, 1232–1244.
(36) Blackledge, M. J.; Brüschweiler, R.; Griesinger, C.; Schmidt, J. M.; Xu, Ping; Ernst, R. R. *Biochemistry*, in press.

Table VII. ^{13}C T_1 Relaxation Analysis for Proline Residues in Antamanide[a]

	NT_1 (two-site jump model) (ms)	NT_1 (correlation function) (ms)	NT_1 (exptl) (ms)
Pro^2			
C$_\alpha$	341 (26)	320 (25)	334
C$_\beta$	552 (83)	545 (75)	570
C$_\gamma$	736 (167)	744 (170)	734
C$_\delta$	398 (28)	430 (17)	426
Pro^7			
C$_\alpha$	340 (26)	316 (27)	318
C$_\beta$	592 (43)	583 (37)	522
C$_\gamma$	867 (89)	859 (33)	790
C$_\delta$	418 (33)	448 (33)	490
Pro^3			
C$_\alpha$	339 (25)	338 (29)	346
C$_\beta$	350 (28)	341 (30)	416
C$_\gamma$	362 (30)	384 (36)	480
C$_\delta$	346 (26)	371 (31)	390
Pro^8			
C$_\alpha$	339 (25)	326 (28)	324
C$_\beta$	349 (25)	333 (28)	356
C$_\gamma$	359 (26)	369 (30)	374
C$_\delta$	346 (26)	359 (30)	366
τ_c (ps)	190 (31)	184 (24)	180[b]

[a] NT_1 relaxation times at 100-MHz ^{13}C resonance frequency are derived from the MD trajectories: (i) based on eq 7 using p_1^{JM}, p_2^{JM}, $\Delta\theta^{JM}$, and τ_{int}^{JM} computed for the two-site jump model and (ii) based on eq 17 using the order parameters S_s^2(CF) and S_f^2(CF) together with τ_{int}^{CF} derived from the correlation function analysis. The overall tumbling correlation time τ_c is obtained by least-squares fitting the computed NT_1 values to the experimental values. The computed values are given as averages over the six trajectories (standard deviations between the trajectories in parentheses). Experimental NT_1 values were determined at 100 MHz and 300 K. [b] Calculated from C$_\alpha$-T_1 relaxation times measured at 125 MHz and 300 K (from ref 36).

tation, are in fair agreement with the experimental data ($\tau_{int} = 30$–36 ps) reported by Mádi and co-workers.[8] For comparison, solid-state NMR investigations of cyclic proline-containing peptides have found internal correlation times of 12 ps for the pucker transition.[34]

For Pro^2 and Pro^7, similar internal correlation times τ_{int}^{CF} emerged from the quantitative evaluation of the time correlation functions for C$_\beta$H, C$_\gamma$H, and C$_\delta$H entities (Table VI). Thus, as expected from the bistable jump model, a single internal correlation time per proline residue characterizes the ring-interconversion dynamics. On the other hand, the correlation times τ_{int}^{CF} deduced for C$_\alpha$H groups in Pro^2 and Pro^7 and all CH groups in Pro^3 and Pro^8 are considerably shorter. Mobility due to rapid local modes rather than the ring-puckering process is the predominant contribution to the reorientation of their CH bonds. The uniformly large values of the order parameters $S^2 = S_f^2 S_s^2$ for Pro^3 and Pro^8 clearly indicate that the motion of the CH bonds is restricted. The motional processes affecting Pro^3 and Pro^8 are not governed by two discrete correlation times but rather by a distribution of short correlation times. Consequently, it is not possible to deduce two well-defined order parameters S_s^2 and S_f^2, and the corresponding values in Tables V and VI should not be overinterpreted.

According to the analysis of Cung and co-workers,[25] who investigated with IR and NMR methods the dynamics of diprolyl sequences in various solvents, the proline dynamic behavior depends on the backbone torsional angle $\phi \approx \chi_0 - 60°$, and a strained conformation ($\phi \approx -80°$) may inhibit the pucker interconversion. This is in accord with crystal data.[35] By restraining the backbone dihedral angles in Pro^3 and Pro^8 to $\phi_{3,8} = -60°$ in simulation G (in unconstrained simulations an average value $\phi_{3,8} = -85°$ was found), the pucker occupancies for these prolines should become similar to those for Pro^2 and Pro^7.[24] Indeed, the computed probabilities p_1^{JM} were 0.28, 0.30, 0.35, and 0.28
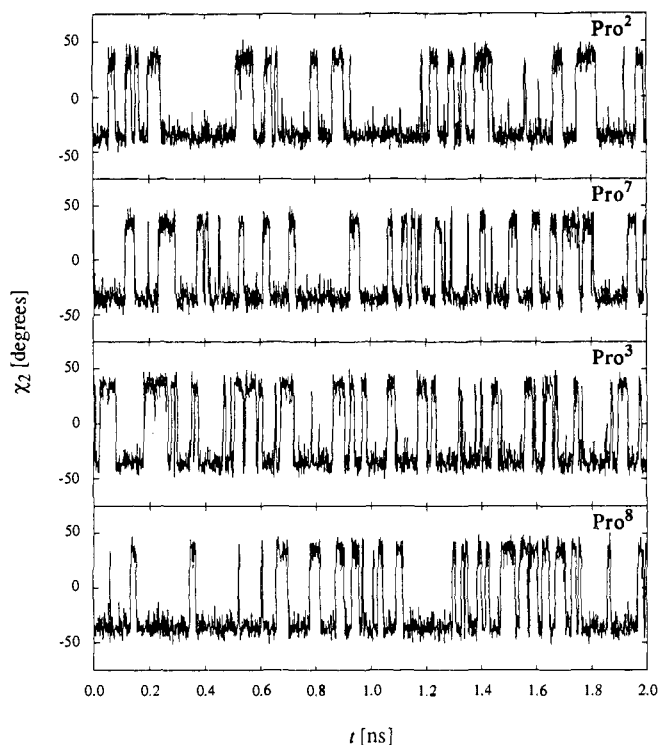
Figure 5. Proline χ_2 dihedral angle trajectories in the LD simulation G of antamanide. The fixed backbone dihedral angles $\phi_{3,8} = -60°$ lead to puckering of all proline residues in contrast to the example shown in Figure 2.

for Pro[2], Pro[7], Pro[3], and Pro[8], respectively (Figure 5). This result confirms the correlation of backbone structure and proline ring mobility. During the 2-ns time span covered by the simulated trajectories, backbone conformational transitions are not likely to happen and have not been observed. Structure refinements[4,6,36] showed that at least two conformations in a dynamic equilibrium are required to represent the antamanide backbone consistently with experimental data. However, a larger number of backbone conformations is not excluded. To account for this, various backbone starting geometries were used in the simulation and found to influence the proline puckering. Pro[2] showed a strong dependence of the ring dynamics on the overall structure. The inaccurate equilibrium distribution of pucker states in Pro[2], found in the simulation, may be due to the omission of solvent effects on the potential of mean force, to the force field parameters, or to incomplete sampling of the configurational space during the simulation. Since the chosen set of starting geometries and their weights are somewhat arbitrary, there is an additional uncertainty in the computed numerical values for the equilibrium distributions and for the exchange rates of the prolines.

Comparison of GROMOS and CHARMM Simulations

In the following, some comments will be made on the similarities and differences that emerged from two LD simulation studies of proline puckering in antamanide using the GROMOS[13] and the CHARMM force field (this work).

Differences in the Procedures. In CHARMM simulations, the molecular conformations are treated in an all-atom model with 162 atoms for antamanide of which 78 are hydrogen, while in GROMOS united atoms are used throughout for apolar CH_n groups, leading to 90 united atoms, of which 6 are exchangeable amide protons. In a first series of simulations, CHARMM version 19 (Brooks et al., 1983) was used where no proline puckering was observed. The final simulations were based on CHARMM version 22. With respect to the earlier force field releases, slight modifications are made in CHARMM 22 concerning the charge separation within the $C_\beta H_2$ methylene entity of proline residues.

In the actual parameter set, carbon and hydrogen atoms bear -0.18 and $+0.09$ unit charges, respectively. The all-atom approach provides an easy possibility of modeling these local electrostatic potentials in contrast to a united-atom model. The new CHARMM force field parameters[10,11] have been developed on the basis of a wide range of ab-initio calculations and experimental data on the structure, dynamics, and thermodynamics of amino acids and of model compounds. For proline, ab-initio calculations were made on N-acetylprolinamide at the 6-31G* level.

The algorithms used for integrating the Langevin equations of motion, the Verlet-type scheme in CHARMM,[19,20] and the leap-frog procedure in GROMOS[37] are slightly different. The terms accounting for atomic friction differ as identical γ values were used for all atoms in the CHARMM simulation, while γ was made dependent on the accessible surface in GROMOS simulations. In GROMOS, the temperature was adjusted by scaling velocity components according to weak coupling to a temperature bath,[38] while in CHARMM the dissipative forces were provided exclusively by the friction term and the temperature enforced by the stochastic term; this is consistent with a stochastic dynamics approach and the applicability of the fluctuation–dissipation theorem.

CHARMM trajectories had to be extended up to 2 ns to achieve constant population ratios for the proline puckering, while 500-ps periods were sufficient in GROMOS simulations due to the faster puckering dynamics. In the CHARMM simulation, the effective residence times were calculated using a threshold angle of $\pm10°$ on the χ_2 value for discrimination of pucker transitions. In the GROMOS investigation, short-lived transitions were discarded if immediate remigration was detected. The two procedures are expected to give similar results when analyzing the same trajectories.

Overall isotropic motional contributions were removed from CHARMM trajectories by orienting the peptide coordinate sets in a principle-axis system. In contrast, individual residue-fixed reference frames were used in the GROMOS analysis, each of which is defined by the triangle formed by the carbonyl carbon nucleus of the respective proline, by the carbonyl carbon nucleus of the preceding residue, and by the center of the proline NC_α bond. This is allowed as long as only the averaging of internal parameters is considered. Time correlation functions for CH bond directors have been computed from the CHARMM trajectories but not from the GROMOS trajectories.

Results. With respect to both proline equilibrium and dynamic properties, the LD simulations revealed significant differences. In the GROMOS simulations, the equilibrium properties of the four prolines qualitatively match the tendencies of the experimental results but show significantly less variation. This contrasts with the CHARMM results which show, in agreement with experiment, that Pro[3] and Pro[8] are essentially confined to a single puckering minimum, while Pro[2] and Pro[7] sample two minima. This is also reflected in the calculated $^3J_{HH}$ coupling constants. In the GROMOS simulations, the dispersion in the population-dependent trans coupling constants is smaller than the experimental one for Pro[3] and Pro[8], while it is larger for Pro[2] and Pro[7]. This can be explained by the pucker state ratios of 1:5 and 1:3 found in GROMOS simulations for the former and latter residues, respectively. In contrast, near equipopulation was found for Pro[2] and Pro[7] in the experiment and in the CHARMM simulations, although in the latter, Pro[2] typically exhibited an inverted population ratio compared to the experimental results. The two pucker states in Pro[3] and in Pro[8] showed a population ratio of 1:40 in the CHARMM simulations. The computed correlation times for proline puckering are shorter than the experimental

(37) Van Gunsteren, W. F.; Berendsen, H. J. C. *Mol. Simul.* **1988**, *1*, 173–185.

(38) Berendsen, H. J. C.; Postma, J. P. M.; van Gunsteren, W. F.; Di Nola, A.; Haak, J. R. *J. Chem. Phys.* **1984**, *81*, 3684–3690.

estimates with both force fields. The dynamics computed by GROMOS simulations is too rapid by a factor of 20–30 compared to the experiment, while with the CHARMM force field, the dynamics appears accelerated by a factor of less than 3; the latter is within the error margins for the experimental correlation times.

The numerical agreement between simulation and experiment with regard to structural properties is similar for the CHARMM 22 and GROMOS force fields. The root mean square (rms) deviation of the computed populations of the two proline conformers from experiment is 0.151 for CHARMM 22 (Table III) and 0.130 for GROMOS (Table II of ref 13). Nevertheless, it is apparent that the CHARMM simulation reproduces qualitatively better the experimental data: The experimental populations are within 0.35 and 0.65 for Pro^2 and Pro^7 and outside of 0.10 and 0.90 for Pro^3 and Pro^8. The CHARMM populations fulfill the same conditions. On the other hand, the GROMOS populations of Pro^2 and Pro^7 spread over a larger interval from 0.25 to 0.75, and for Pro^3 and Pro^8 they are outside of the smaller internal 0.17 to 0.83. The contrast between the behavior of Pro^2, Pro^7 and Pro^3, Pro^8 is smaller in the GROMOS simulation than in the experiment and in the CHARMM results. The rms deviation of the computed proline χ_i angles, $i = 0$–4, from experiment is 9.0° for CHARMM 22 (Table II) and 9.7° for GROMOS (Table II of ref 13). Both CHARMM 22 (Table IV) and GROMOS (Table III of ref 13) yield an rms deviation of computed $^3J_{HH}$ values from experiment of 1.5 Hz; although, in GROMOS the proton dihedral angles had to be estimated from the carbon and nitrogen dihedral angles.

To avoid biased results from inadequate sampling of the backbone dynamics of antamanide, a set of six starting structures was used to initiate the CHARMM simulations. In fact, proline puckering was found to depend on the backbone conformation, which did not undergo a transition during the time covered by the trajectories. The result is in agreement with experiment where the backbone interconversion time is on the order of microseconds. This behavior is in contrast to the occasional conformational transitions of the peptide backbone in GROMOS simulations and to the absence of a significant influence of the sampled peptide

ring conformations on the proline dynamics. Further constraining of the backbone conformation would certainly affect the proline dynamics also in GROMOS simulations.

Overall, the new all-atom CHARMM 22 potential energy function provides a realistic description of the equilibrium and dynamics of proline rings. Since prolines play many important roles in biological systems, such accuracy is of general utility in studies of peptides and proteins by force-field calculations.

Conclusions

The proline conformation and pucker dynamics in the cyclic decapeptide antamanide have been simulated using the classical molecular dynamics program CHARMM with the CHARMM 22 potential energy functions. The structural results are in good agreement with experimental NMR-based structure information. Pro^2 and Pro^7 show dynamic averaging effects, while Pro^3 and Pro^8 exhibit the experimentally observed rigidity. Also, the equilibrium structural parameters such as homonuclear J coupling constants and carbon-13 longitudinal relaxation times are reproduced correctly by the simulation. The time scale for the internal motion processes was found to be somewhat shorter than the experimental NMR estimates. However, the error margin of the data is such that the deviation may not be significant. A correlation between the puckering process and the peptide ring backbone conformation was demonstrated by MD simulation in agreement with earlier experimental results reported on diprolyl sequences.[25]